Fatigue of crystallizable rubber: Generation of a Haigh diagram over a wide range of positive load ratios

Clément Champy, V. Le Saux, Yann Marco, Thomas Glanowski, Pierre Charrier, Wilfried Hervouet

Fatigue of crystallizable rubber: generation of a Haigh diagram over a wide range of positive load ratios.

C. Champy[a,b], V. Le Saux[a,*], Y. Marco[a], T. Glanowski[a], P. Charrier[b], W. Hervouet[b]

[a] *ENSTA Bretagne – Institut de Recherche Dupuy de Lôme (IRDL), UMR CNRS 6027, Brest, France*

[b] *Vibracoustic – CAE Durability Prediction Department, Carquefou, France*

Abstract

A Haigh diagram is built for a carbon black filled rubber blend that exhibits Strain Induced Crystallization (SIC) for a wide range of positive displacement ratios. A strategy for the initiation detection, which becomes difficult for high displacement ratios, is proposed and validated thanks to regular visual follow-up. Some experimental cautions are taken to avoid any temperature and strain rate effects on the results, more specifically on the strain induced crystallization phenomenon. It is found that a reinforcement related to strain induced crystallization is present for load ratios (up to displacement load ratio of 0.35). For higher load ratios, the reinforcement effect reduces leading to a Haigh diagram that looks like a bell, as already shown by Cadwell *et al.* (S. Cadwell, R. Merrill, C. Sloman, F. Yost, Dynamic fatigue life of rubber, Industrial and Engineering Chemistry 12 (1940) 19–23).

Keywords: strain induced crystallization, crystallizable rubber, fatigue, haigh diagram, reinforcement

*Corresponding author. Tel.: +33 (0)2 98 34 87 18; Fax: +33 (0)2 98 34 87 30
URL: vincent.le_saux@ensta-bretagne.fr (V. Le Saux)

Introduction

Rubber-like materials are commonly used in the automotive industry due to their ability to undergo large deformations without important permanent set and to their damping properties, which make them appropriate candidates for anti-vibration parts. In service, these parts are submitted to complex cyclic loadings with significant variations of the mean and amplitude loadings (see Figure 1a for an example). Therefore, a good design against fatigue for various load ratios is mandatory to ensure the reliability of these parts (see Figure 1b). Moreover, the current trend for automotive anti-vibration parts is to increase the swaging applied to outer inserts (see Figure 1c), which leads to higher pre-strain values for unloaded parts. This implies to enlarge the experimental fatigue database needed to design the parts, especially for positive high load ratios.

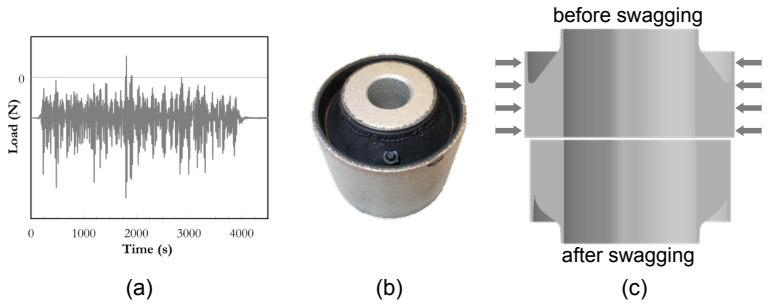

Figure 1: Example of a complex cyclic loading (a), of industrial part with high swaging (b) andtypical half cross-section before and after the swaging (c).

The effect of the mean amplitude on the fatigue life is usually evaluated thanks to the classical Haigh diagram which plots lifetime isocurves in the

mean-amplitude strain/stress plan. More than 70 years after its publication, the work of Cadwell *et al.* [1] still remains a reference. The original diagram proposed by the authors is presented on Figure 2a. As the results are not presented in a conventional way (fatigue life as a function of the minimum strain for different strain amplitude), they are replotted on Figure 3 using classic axes (strain amplitude as a function of the mean strain for different fatigue lives).

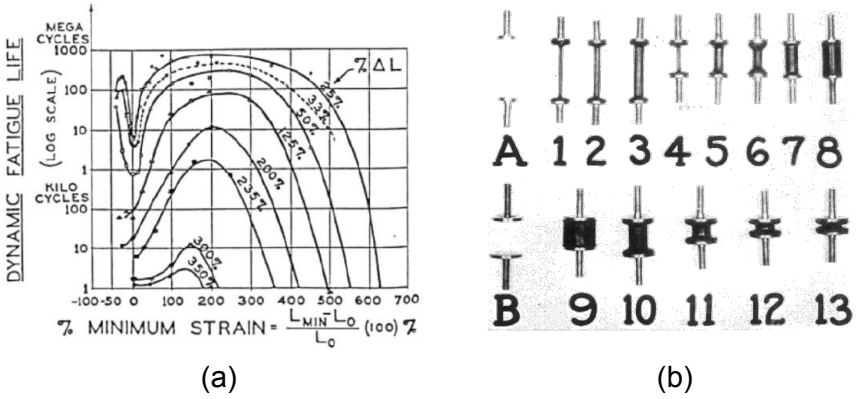

Figure 2: Cadwell *et al.* [1] fatigue results (a) and geometries of the specimens (b).

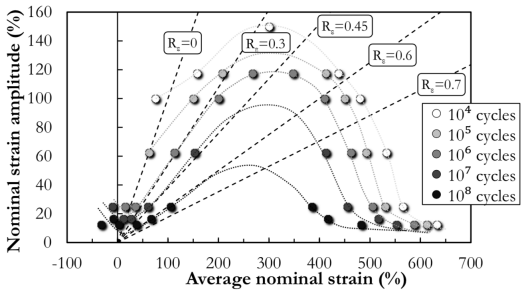

Figure 3: Haigh diagram associated to the original results of Cadwell *et al.* [1].

The reasons behind the fact that Cadwell *et al.* still remains a reference

nowadays are simple: the experimental database is huge (about 450 tests), covers a wide range of load ratio and the results are quite astonishing. Actually, the tension-tension area of the Haigh diagram can be divided into two regions. The first one corresponds to small load ratio where a reinforcement phenomenon is noticed and characterized by a positive slope of the iso-duration life curves. This means that an increase of the mean loading leads to an improvement of the fatigue life. Beyond a given mean strain, the reinforcement decreases and the slopes become negative: an increase of the mean strain leads, in this range, to a reduction of the fatigue life.

The origin of this reinforcement is related to the strain induced crystallization phenomenon (SIC) [2, 3]. The crystallites which are created during the fatigue cycles can cumulate over the cycles under positive load ratio, so-called non relaxing cycles [4]. If the crystallites amount becomes high enough, they are considered to act as a barrier to the propagation of small fatigue cracks [5–9], leading to a "dentelle" effect [10] or knotty tearing [5]. However, there are some points that are questionnable regarding Cadwell *et al.* [1] approach:

- The number of sample geometry (as high as 13, see Figure 2b). Fatigue is known to be influenced by the volume effect [11], meaning that the measured number of cycles can be dependent on the specimen geometry. This effect is related to the higher probability of finding a defect leading to failure with increasing loaded volume.

- The frequency was adapted to minimize the testing duration. Frequencies up to 60 Hz were used. Nevertheless, strain induced crystallization depends on time and temperature [3, 12–14]. High frequencies can

prevent the occurence of strain induced crystallization due to excessive strain rate, or because of the temperature rise induced by heat build-up [12, 15–17] which melts the already existing crystallites.

- The fatigue end of life criterion used is the total fracture of the specimen. Besides the fact that this criterion is questionnable regarding the industrial applications, it also increases significantly the testing duration, especially for high load ratios. This criterion is also questionnable from a scientific point of view as it may become really difficult to fully break a sample due to the branching phenomenom that occurs at the crack tip [6, 7, 9], as it induces a reduction of the resisting section and some local redistribution of the strains and stresses, leading to an increase of the crystallization. Moreover, this criterion leads to fatigue lives that are dependent on the specimen geometry and load ratio, as the proportion between initiation and propagation are different ;

- The strain is evaluated from the macroscopic displacement and no local evaluation is performed. The application of these results to other geometries is therefore limited and the strain levels evaluated are questionable since some complex geometries are used.

Late after the pioneer work of Cadwell *et al.* [1], some authors tried to build a Haigh diagram for different types of rubber matrix and fillers [7, 8, 18–22]. They improved the experimental settings defined by Cadwell *et al.* by using a single sample geometry submitted to cyclic loading with a limited frequency (to prevent from too high heat build-up). The end of life is based on the initiation of small fatigue cracks or on a stiffness drop.

However, besides these significant improvements, all these studies share the same limitation: the positive load ratios are kept below 0.3, therefore only a small area of the Haigh diagram is investigated. Consequently, similar results to the ones of Cadwell *et al.* are not available in the literature.

The aim of this paper is to build a full Haigh diagram, describing a large range of positive load ratio (for tension-tension loads) with well mastered experimental conditions. The paper is divided into 4 sections. In section 1, the experimental settings are described. Then, the end of life detection criterion is presented in section 2. Section 3 is dedicated to the validation of the evaluation of the local strain from the macroscopic displacement. Finally, the obtained Haigh diagram covering the full tension-tension conditions is presented in section 4, both in terms of macroscopic displacements and local strains.

1. Experimental settings

1.1. Material and samples

The material studied is a a carbon black filled NR (Natural Rubber) / IR (Isoprene Rubber) blend whose recipe is given in table 1. The specimen used is obtained by injection process to be representative of the automotive anti vibration parts. Its geometry, called AE2, is given in Figure 4. It has been chosen for several reasons. The first one is related to the section reduction that acts as a stress and strain concentrator. It is therefore possible to reach high strain values for limited macroscopic displacement. Moreover, the fatigue crack initiation occurs in the notched area systematically. Then, the

component	content [phr]
NR	75
IR	25
zinc oxide	4.1
plasticizer	7
carbon black (N339)	29
stearic acid	2
antioxidant	3
antiozonant	3
accelerator	1

Table 1: Recipe of the material

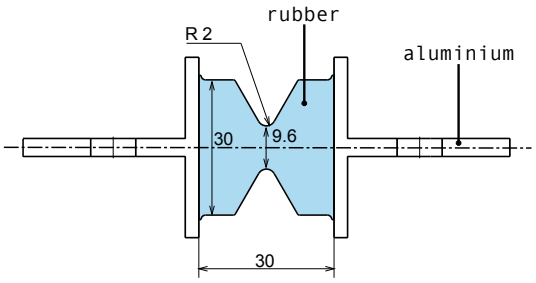

Figure 4: AE2 specimen. The dimensions are given in mm.

gauge part of the sample is limited, as well as the affected volume. This helps limiting the heat build-up during the fatigue tests. Moreover, as the section in the central zone of the specimen is small, the heat build-up difference between the skin of the specimen and its bulk will be limited, leading to small temperature gradients.

1.2. Test procedure

All experiments were performed on a pneumatic test rig already presented by Ostoja Kuczynski *et al.* [23] and were displacement controlled. The load ratio, $R_d = d_{\min}/d_{\max}$ is computed based on the minimum and maximum displacements over one cycle. All the tests are performed in a thermal oven whose temperature is regulated at 23°C. In order to limit the heat build-up that may influence strain induced crystallization [12, 13], the testing frequencies are adapted between 0.75 and 8Hz depending on the testing condition in order to keep the same order of magnitude of heat build-up. Figure 5 presents the maximum heat build-up measured by an infrared pyrometer at the skin during the fatigue tests. A maximum value of 8°C is observed, leading to a maximum heat build-up at the core evaluated to 10°C [17, 24]. This limited temperature rise have a very limited impact on the capacity of the material to crystallize under strain [12, 13]. Moreover, the frequencies remains low enough to neglect the strain rate effect on the SIC [3, 13, 14]. Finally, even for the longest duration (13 days), the in-situ ageing induced by the temperature can be neglected [25–27].

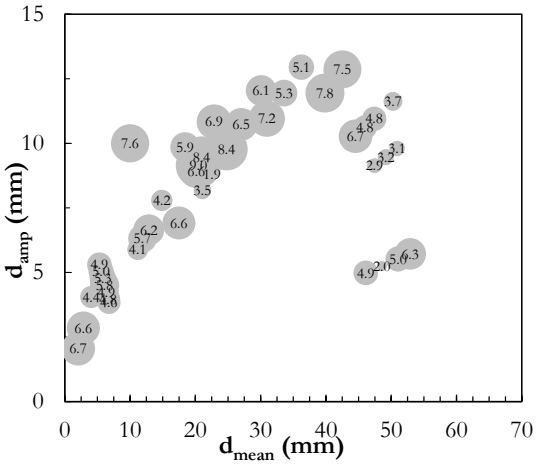

Figure 5: Maximum heat build-up measured on the external surface of the specimen for a wide range of test. The maximum heat build-up encountered is 8°C and the mean heat build-up is around 5 °C.

1.3. Optical measurements

The images of the cracks at the samples' surface were taken with a standard DSLR[1] camera equiped with a 50 mm lens. The stereo Digital Image Correlation (DIC) measurement has been performed thanks to a VIC-3D system developped by Correlated Solutions that relies on two 2.3MPixels Grasshoper monochromatic cameras (model PointGrey GS3-U3-23S6M-C), both equipped with a 28 mm lens.

2. Definition and validation of an initiation criterion

One major difficulty for approaches based on fatigue crack initiation is the experimental detection of the macroscopic initiation. Three main approaches can be found in the literature.

[1]Digital Single Lens Reflex

2.1. Criteria from the literature

2.1.1. Total fracture

The first criterion is based on the total fracture of the specimen. Cadwell *et al.* [1] were amongst the first to use such a criterion. Its use can be questionnable regarding the industrial applications (besides being also questionnable from a scientific point of view), especially the automotive industry. This criterion is specimen dependant, explaining why its use is rather seldom nowadays [22, 28, 29].

2.1.2. Optical detection

The second criterion is based on the detection of a crack of a given size. Many authors have used such an approach [6, 19, 30]. The main drawbacks are the objective definition of a critical macroscopic crack size and the necessity of a constant follow-up of the test in order to know precisely when to stop it. Moreover, depending on the location of the crack(s), the camera may not be looking at the correct location, and cracks may be missed.

2.1.3. Variation of a mechanical variable

The last criterion is based on the variation of a macroscopic quantity, such as the load [31, 32] or the secant stiffness [23]. The main advantages are the easy instrumentation and the fact that the number of cycles can be evaluated after the end of the test. However, the results are conditionned by the sample geometry and the post-processing may have to be adapted from one geometry to another.

2.2. Choice of a criterion related to the non-viscous contribution of stiffness decrease

In this study, we have chosen the last category of criterion and more specifically the one of Ostoja-Kuczynski *et al.* [23] since a correlation between the variation of the stiffness drop rate and the appearance of a macroscopic crack has been demonstrated. The fatigue end of life is defined as the number of cycles needed to observe a fixed drop of the cyclic stiffness of the sample K, defined as:

$$K = \frac{F_{\max} - F_{\min}}{d_{\max} - d_{\min}} \tag{1}$$

The quantity is monitored cycle by cycle. The criterion assumes that the stiffness evolution is mainly related to two phenomena : the viscoelasticity and the growth of defects. The dependency of the stiffness to the viscoelasticity can be modelled with a logarithmic function. The end-of-life is then reached when the experimental stiffness deviates from the modelled stiffness. From a mathematical point of view, this leads to a simple, yet efficient, initiation criterion:

$$N\frac{\mathrm{d}K}{\mathrm{d}N} \neq c_{\mathrm{cst}} \tag{2}$$

A complete demonstration can be found in Ostoja-Kuczynski *et al.* [23]. The authors have also shown that this criterion corresponds to a total crack length of around 1 to 2 mm for the AE2 sample for relaxing testing conditions.

2.3. Validation of the criterion for non relaxing conditions

The criterion was designed for relaxing cyclic loading conditions and has not been challenged yet for non relaxing testing conditions. In order to check

its relevancy for such loading conditions, a specific test campaign was conducted. Various different R_d ratios were chosen in accordance with the range of interest for the Haigh diagram ($R_d \in [0.3; 0.82]$). Figure 6 presents the evolution of the normalized stiffness, *i.e.* divided by the first cycle stiffness, during the fatigue test for the considered load ratio. Starting with the evo-

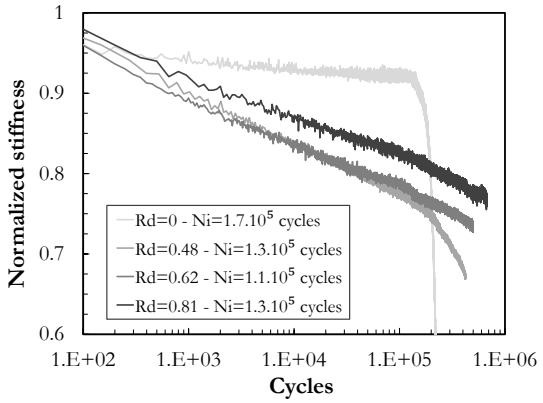

Figure 6: Evolution of the normalized stiffness for various load ratio.

lution of the stiffness for the relaxing tests ($R_d = 0$), we can notice an initial linear loss of stiffness (in log scale), related to viscoelastic phenomena. Beyond a certain number of cycles (around $1.5 \cdot 10^5$ cycles), the stiffness loss increases significantly and can be related to the propagation of a macroscopic crack. In that case, the macroscopic initiation can be easily identified and related to the non viscoelastic decrease of the stiffness. For the other experiments (R_d values of 0.48, 0.62 and 0.81), the stiffness drop is far less significant, but still visible and the same initiation criterion can be used. To check the relevancy of this criterion and relate the number of cycles to initiation to macroscopic damage, some pictures were taken for several number of cycles for various load ratios (Figure 7).

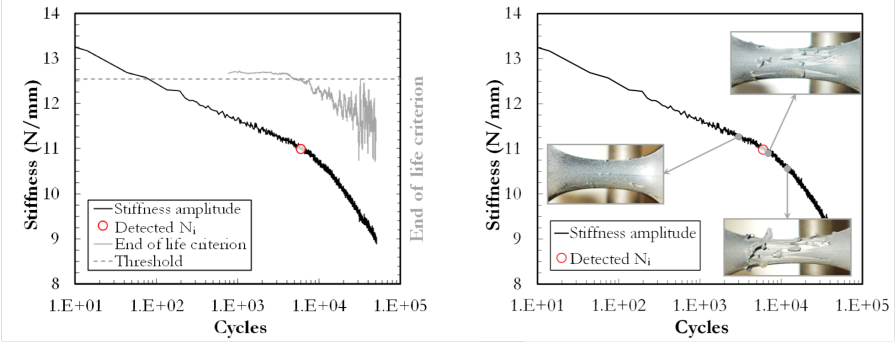

(a)

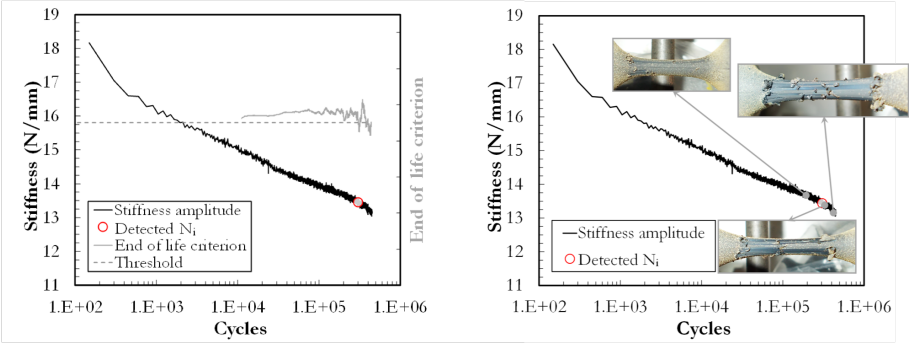

(b)

Figure 7: Stiffness variation and evolution of the criterion for along $R_d = 0.3$ (a) and $R_d = 0.48$ (b).

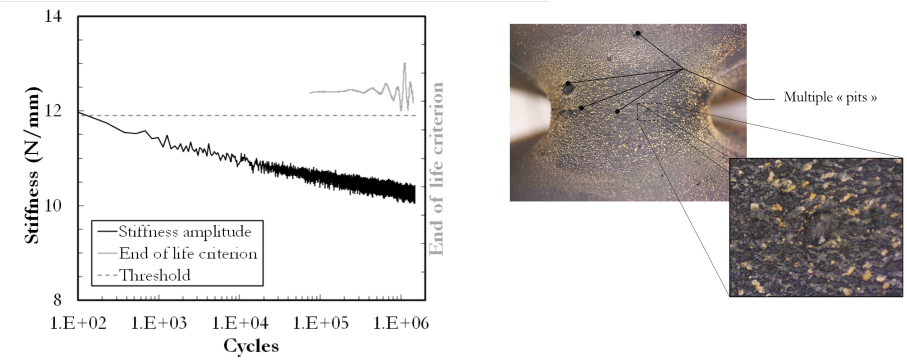

Figure 8: Stiffness variation and evolution of the criterion along a test (a) and evolution of the the outer surface (b) for $R_d = 0.31$.

As for relaxing conditions, microscopic cracks appear long before the macroscopic initiation [33] and their number increases with the number of cycles. For relaxing conditions, these cracks propagate in a direction that is perpendicular to the loading direction. However, for the considered positive load ratios, these microscopic cracks propagates in a parallel direction to the tensile direction before becoming fully relaxed, leading to the stop of their propagation. Figure 8 shows the outer surface of the specimen for a test that has been stopped after $1.5 \cdot 10^6$ cycles (the initiation criterion is not met). A significant number of small cracks whose size are close to a few dozens of micrometers, are visible, but they do not propagate similarly to the mechanisms highlighted in Figure 7 and have no effect on the stiffness of the sample. These results show that we are still sensitive to stiffness drop, even for high positive load ratio, and able to capture a nonlinear drop. Finally, significant cyclic stress relaxations can occur during the test, especially for very high load ratio, that may influence the measured number of cycles to initiation. To evaluate the importance of such phenomena, fatigue tests were performed for a given mechanical loading condition for various frequencies (1, 2 and 5 Hz), thus different experimental strain rates. The results are presented on Figure 9, where the fatigue life and the maximum skin temperature measured in the thinnest section of the specimen are reported as function of the strain rate. The strain rate $\dot{\varepsilon}$ is estimated from the maximum nominal strain range $\Delta\varepsilon$ and the testing frequency f_r according to $\dot{\varepsilon} = f_r \Delta\varepsilon$. One can see that the higher the strain rate, the higher the skin temperature. However, the fatigue lives are very comparable which tends to prove that the heat build-up and the cyclic stress relaxation do not influence the estimation of the fatigue life.

This conclusion stands of course only for the considered testing conditions and may change if significant higher frequencies are applied.

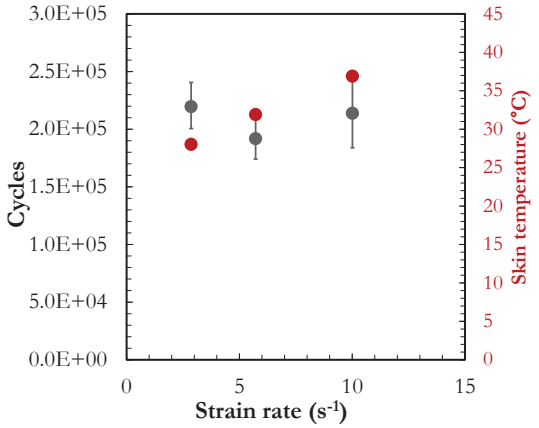

Figure 9: Effect of the testing frequency on the fatigue life based on the end-of-life criterion in the case of a non relaxing test defined by $\varepsilon_{mean} = 322\%$ and $\varepsilon_{amp} = 72\%$ corresponding to a load ratio $R_\varepsilon = 0.64$.

3. From global displacement to local strain

Due to its complex geometry, the evaluation of the local strain is not direct and requires a dedicated conversion rule. The strategy proposed here consists in evaluating numerically this conversion rule thanks to FEA simulations, and to validate it experimentally using Digital Image Correlation.

3.1. Evaluation of the conversion rule

As very high strain level needs to be reached, the constitutive behavior law needs to be chosen carefully. We chose an hyperelastic modelling approach and used the Edwards-Vilgis potential [34] which presents the ability

to capture the stiffening phenomenon at high strain due to the finite extensibility of the macromolecules for a limited number of parameters. Its expression is given by:

$$
\begin{aligned}
W = \frac{N_c^\star}{2}\left[\frac{(1-\alpha^2)\sum_{i=1}^{3}\lambda_i^2}{1-\alpha^2\sum_{i=1}^{3}\lambda_i^2} + \ln\left(1-\alpha^2\sum_{i=1}^{3}\lambda_i^2\right)\right] \\
+ \frac{N_s^\star}{2}\left[\frac{(1-\alpha^2)(1+\eta)}{1-\alpha^2\sum_{i=1}^{3}\lambda_i^2}\sum_{i=1}^{3}\frac{\lambda_i^2}{1+\eta\lambda_i^2}\right. \\
\left. + \ln\left(1-\alpha^2\sum_{i=1}^{3}\lambda_i^2\right) + \sum_{i=1}^{3}\ln\left(1+\eta\lambda_i^2\right)\right]
\end{aligned}
\tag{3}
$$

This model has 4 parameters, $N_c^\star$, $N_s^\star$, η and α. $N_c^\star$ is related to the permanent crosslink density, $N_s^\star$ is related to the entanglements density, η is used to model the friction in the entanglements and α is related to the chains locking stretch ($\alpha = 0$ would model a Gaussian network). The components λ_1^2, λ_2^2 and λ_3^2 are the principal streches. Although this model relies on physical foundations, the values of the parameters will not be discussed. This model was chosen here for its prediction capabilities associated with its very limited number of parameters. These parameters have been identified using a Levenberg-Marquardt optimization algorithm from the macroscopic displacement-force curve obtained on the AE2 sample. We chose to identify these parameters using the same specimen to avoid any process effect that could lead to small variations of the materials properties. The simulations were done using the Finite Element Software Abaqus and the hyperelastic potential was implemented using a fortran user subroutine. Some elements of the implementation are given in [35]. A cyclic curve was first generated as shown in Figure 10. Several increasing displacement increments were chosen. For each maximum displacement, the stabilized state was reached after 5 cy-

cles and the maximum force/displacement point obtained for the last cycle was added to the identification database. This experimental cyclic hyperelastic response was then used to identify the parameters of the constitutive model. Figure 10 presents a comparison between the experimental and the numerical results. The excellent agreement confirms that the chosen hyperelastic potential is able to capture the nonlinear behaviour of the curve and can cover a large range of strain, compatible with the one encountered during the tests. The values of the optimized parameters is given in Table 2.

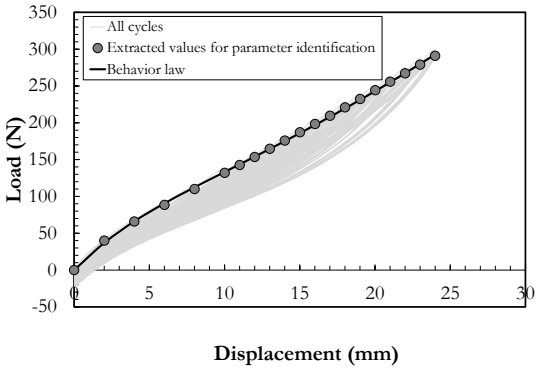

Figure 10: Identification of the hyperelastic parameters.

parameter	value
$N_c^\star$	0.61 MPa
$N_s^\star$	0.50 MPa
η	0.50
α	0.15

Table 2: Set of parameters of the Edwards-Vilgis identified from the cyclic test performed on the AE2 specimen.

The conversion rule can then be established thanks to a FEA simulation. A polynomial relation is used to relate the highest maximum principal strain to the macroscopic displacement.

3.2. Validation of the conversion rule

Once the hyperelastic model is identified, the conversion rule relating the displacement to strain can be evaluated. The considered strain here is the maximum principal strain, *i.e.* $\max_{i\in[1,2,3]}(\lambda_i) - 1$. The displacement, resp. the maximum principal strain, is computed at the node located in the thinnest section of the specimen, resp. on the centroid of the element in the thinnest section of the specimen, and on the free surface. The results are presented in Figure 11. A validation of the conversion rule, based on the use of Stereo Digital Image Correlation is proposed here. A speckle pattern is first applied on the specimen and a cyclic test to accomodate the Mullins effect is applied for a displacement corresponding to 85% of the strain at break. The displacements are then measured during the loading step of the stabilized cycle and the strains are computed from the displacement fields. Figure 11 presents a comparison between the conversion rule obtained from the FEA and from the experiments. A very good agreement can be observed. Therefore, the displacement to strain conversion rule evaluated using the numerical model is validated and will be used in the following to evaluate the local strain from the global displacement. This conversion rule is therefore a key element in the transcription of the measured global Haigh diagram (in displacement) to the evaluated local Haigh diagram (in strain).

Once the conversion rule has been established and validated, it can be used to convert the minimum, resp. maximum, displacement d_{min}, resp.

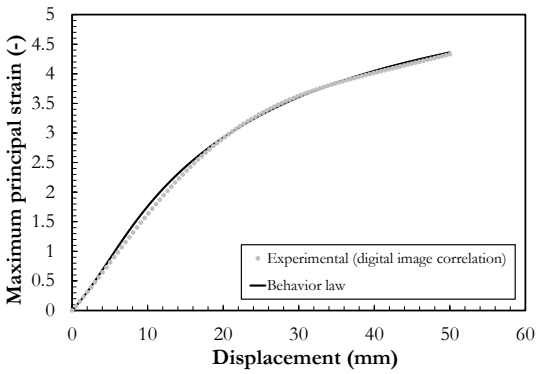

Figure 11: Comparison between the experimental and the numerical displacement/strain conversion rule.

d_{max}, over the cycle into local minimum, resp. maximum, strain ε_{min}, resp. ε_{max} (according to the definition given above). A mean strain and an amplitude strain can then be computed according to $\varepsilon_{mean} = 0.5 \cdot (\varepsilon_{max} + \varepsilon_{min})$ and $\varepsilon_{amp} = 0.5 \cdot (\varepsilon_{max} - \varepsilon_{min})$.

4. Haigh diagram

4.1. Using macroscopic displacement

A large number of samples have been tested (132) for various load ratios ($R_d = 0, 0.3, 0.38, 0.43, 0.47, 0.54, 0.62, 0.68$ and 0.8) and various frequencies (see Section 1.2). For each load ratio, several maximum displacements were chosen. For each loading condition, at least 3 samples were tested and a mean value was computed. Based on these information, it is possible to build the isolifetime lines in the Haigh diagram (see Figure 12). The experimental data are plotted using full markers. The darker the color of the marker, the shorter the fatigue life. The global "bell" shape, already highlighted by Cadwell *et al.* is clearly visible. The iso lifetime curve presents first a

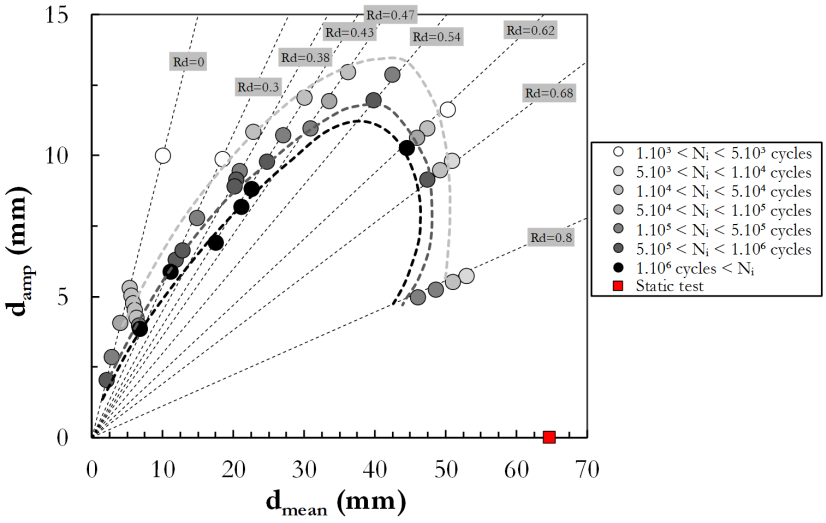

Figure 12: Haigh diagram in the space: mean displacement – displacement amplitude.

positive slope leading to the so-called reinforcement phenomenon for load ratios $R_d \in [0; 0.54]$, then a negative slope for $R_d \in [0.54; 0.8]$, meaning the reinforcement phenomenom is no longer effective. These observations are very similar to the ones of Cadwell *et al.* However, we can notice that the static failure point does not match with the cyclic data. This result can be explained by the fact that the results are plotted in terms of displacement, onis is a macroscopic quantity that is not representative of the local strain in the center of the specimen. It is therefore mandatory to compute the local strain from the macroscopic displacement. Moreover, we can also notice significant negative slopes beyond a load ratio close to 0.5, that may be corrected by the transcription of the displacement Haigh diagram to a strain Haigh diagram. Finally, it should be underlined that a total of 132 specimens were used for the generation of this curve (only the mean points are plotted), for a total experimental time evaluated at 9 months.

4.2. Using local maximum principal nominal strain at failure location

Based on the Haigh diagram presented in section 4.1 and on the displacement-strain conversion rule established in section 3.1, it is possible to convert the Haigh diagram written in displacement as a Haigh diagram written in terms of nominal strain. This plot is shown in Figure 13. The same styles are used here: the darker the marker, the longer the fatigue lifetime. As a first

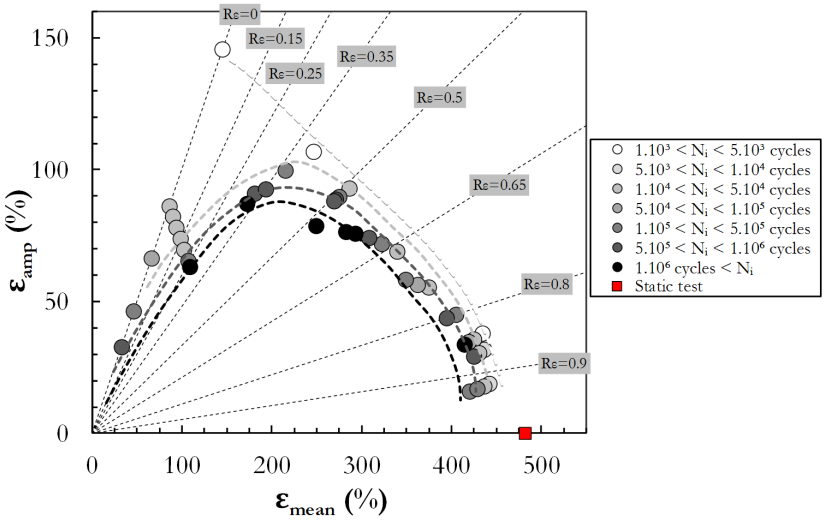

Figure 13: Haigh diagram in the space: mean maximum principal nominal strain – maximum principal nominal strain amplitude.

remark, we can still notice the presence of the bell shape of the isolifetime curves, as for the displacement Haigh diagram (see Section 4.1). We can also see that the static failure strain is now consistent with the fatigue data. The negative slopes are now lower, which changes the overall aspect of the curves, with a smoother transition between a reinforcement defined with a positive slope, and the loss of the reinforcement defined by the negative slope at a load ratio value of 0.35. The overall shape of the Haigh diagram is consistent

with the results of Cadwell *el al.* (see Figure 3). However, we can notice that, due to the shape of the displacement to strain conversion rule, a slight change of the strain levels can induced significant changes in terms of fatigue life. This is especially noticable at high load ratio, as the markers filled with the shade of gray (corresponding to different level of fatigue life) are almost grouped together. It is therefore really important to characterize the fatigue properties with a large number of specimen and loading conditions, if we want to get reliable data that can be used to design industrial parts under non relaxing testing conditions. The proximity of the isolifetime curves has not been observed on Cadwell *el al.* results. There are at least two reasons. The first one is that no local strain evaluation was performed by Cadwell, and strains were estimated from the global displacement applied to the specimen. On some geometries (see Figure 2-b), this could be justified but for other geometries, this choice is very questionnable. This is especially true for these specimen geometry as the displacement to strain conversion rule may be highly nonlinear, as in our case (see Figure 11). This could reduce the gap between each isolifetime curve. The second one is related to the end-of-life criterion (initiation in our case versus fracture for Cadwell). If fracture was considered as end-of-life criterion in our case, longer duration lives would be obtained, especially for testing conditions that lead to very high fatigue life. This would impact the distance between each isolifetime curve, without changing the overall shape of the curves. Finally, the comparison between the two Haigh diagrams shows that, even if some points are questionnable regarding the choices of Cadwell *et al.*, the results are consistent with ours and clearly highlight the significant role of strain induced crystallization on the

reinforcement phenomenon [6–8]. The connection between this reinforcement and SIC has not been explicitely proved here, and X-ray diffraction measurements still need to be performed, for testing conditions consistent with the one chosen here. Finally, it should be underlined that the obtained Haigh diagram is dependent on the compound used, the local stress and stress state and the value that is used to build the Haigh diagram (maximum principal strain). Careful verifications should be performed to check the transposition of the proposed results to another configuration (compound, specimen geometry and local strain/stress state).

Conclusions

A complete Haigh diagram has been generated for a wide range of positive load ratio under tension/tension loading. A rigorous experimental campaign has been set-up. The test frequencies were carefully selected in order to prevent a too high heat build-up and to high strain rates, that may influence the SIC, and thus the reinforcement phenomenom under cyclic loading. The fatigue life was defined using a criterion based on the drop of stiffness rate. This approach was originally set-up for relaxing fatigue tests and a study was performed to assess the reliability of the initiation criterion to non relaxing testing conditions. To do that, some pictures, taken with a DSLR at various number of cycles during the tests, have shown that this stiffness drop can be related to the apparition of macroscopic cracks or peels when the load ratio increases. A conversion rule was established to convert the macroscopic displacement into a local strain based on numerical simulations validated with stereo Digital Image Correlation. These results allowed us to obtain

an extensive Haigh diagram (132 specimens used, 280 days of test) plotted both in displacements and more importantly in strains. This Haigh diagram covers a wide range of positivite load ratio for tension-tension loadings (from 0 to 0.81). This kind of result, rare in the literature, clearly highlights the significant role of the strain-induced crystallization on the fatigue life of crystallizable rubber-like materials and the necessity to have access to such data for the fatigue design of structure submitted to complex variable loading. However, direct strain induced crystallization measurements, using X-ray diffraction for example, would be very useful to prove in a more direct way the connection between the bell-shaped Haigh diagram and the strain induced crystallization.

Acknowledgements

The authors would like to thank the French Minister for Research (ANRT) for its financial support (CIFRE 2012/0724) and the reviewers for their careful reading, which helped to improve the paper.

Appendix A. Experimental data

The experimental data is provided in this section. To keep the size of the data reasonable, only the mean fatigue life is provided, as well as the standard deviation (when the number of data is sufficient to evaluate a relevant value).

Displacement [mm]			Strain [%]			Duration life [cycles]	
d_{min}	d_{max}	R_d	ε_{min}	ε_{max}	R_ε	mean	std
0	20	0	0	291.1	0	1 411	216

8.56	28.28	0.303	139.9	353.5	0.396	4 326	1 455
38.64	61.89	0.624	397.1	472.6	0.840	4 699	–
47.19	58.63	0.805	424.2	461.4	0.919	8 616	460
41.10	60.70	0.677	405.1	468.5	0.865	9 731	5 221
0	10.60	0	0	172.1	0	12 361	3 232
0.53	10.60	0.050	7.9	171.1	0.046	16 886	3 129
36.44	58.34	0.625	389.6	460.5	0.846	19 882	7 194
1.06	10.60	0.100	16.1	172.1	0.093	21 206	5 016
1.59	10.60	0.150	24.4	172.1	0.142	21 452	5 921
18.03	42.12	0.428	270.6	408.4	0.663	28 641	6 535
12.03	33.70	0.357	193.6	379.2	0.511	30 374	14 291
45.52	56.57	0.805	419.0	454.5	0.922	36 971	24 693
39.70	58.63	0.677	400.6	461.4	0.868	39 382	24 475
23.28	49.18	0.473	320.0	430.5	0.743	43 357	6 378
2.12	10.60	0.200	32.9	172.1	0.191	47 816	13 633
0.00	8.10	0	0	132.4	0	61 872	9 960
21.63	45.52	0.475	306.5	419.0	0.731	96 207	40 994
35.34	56.57	0.625	385.6	454.5	0.848	90 949	24 297
16.29	37.76	0.431	250.6	394.2	0.636	132 049	24 053
41.12	51.09	0.805	405.2	436.6	0.928	137 666	10 254
43.32	53.82	0.805	412.1	445.4	0.925	149 379	–
7.07	22.65	0.312	115.4	314.9	0.366	198 656	39 923
0	5.7	0	0	92.5	0	217 567	28 247
29.66	55.39	0.536	360.9	450.6	0.801	220 162	50 804
11.48	30.39	0.378	185.5	364.6	0.509	352 297	156 736

19.99	41.90	0.477	291.0	407.7	0.714	331 199	74 316
2.65	10.60	0.250	41.5	172.1	0.241	485 805	49 726
11.32	29.61	0.382	183.0	360.6	0.507	567 882	42 303
38.3	56.57	0.677	396.0	454.5	0.871	638 724	320 314
5.58	18.20	0.306	90.4	272.5	0.332	640 730	99 511
27.90	51.79	0.539	351.3	438.8	0.801	681 727	132 333
15.00	34.54	0.434	234.5	382.5	0.613	687 449	61 678
6.22	19.52	0.319	101.2	286.3	0.353	830 241	299 710
0.00	4.10	0	0.0	65.6	0	1 018 307	438 213
11.23	29.06	0.386	181.6	357.7	0.508	934 254	–
12.90	29.25	0.441	206.1	358.8	0.574	$> 1\,000\,000$	–
34.25	54.80	0.625	381.4	448.7	0.850	$> 1\,000\,000$	–
2.92	10.60	0.275	45.9	172.1	0.267	1 040 250	246 131
10.56	24.39	0.433	171.5	328.5	0.522	$> 1\,100\,000$	–
13.74	31.35	0.438	217.7	369.1	0.590	$> 1\,300\,000$	–
5.28	17.05	0.310	85.4	259.5	0.329	$> 1\,500\,000$	–

Table A.3: Experimental results.

[1] S. Cadwell, R. Merrill, C. Sloman, F. Yost, Dynamic fatigue life of rubber, Industrial and Engineering Chemistry 12 (1940) 19–23.

[2] B. Huneau, Strain induced crystallization of natural rubber: a review of X-ray diffraction investigations, Rubber Chemistry and Technology 84 (2011) 425–452.

[3] N. Candau, L. Chazeau, J. Chenal, C. Gauthier, J. Ferreira, E. Munch,

C. Rochas, Characteristic time of strain induced crystallization of crosslinked natural rubber, Polymer 53 (2012) 2540–2543.

[4] S. Beurrot-Borgarino, B. Huneau, E. Verron, P. Rublon, Strain-induced crystallization of carbon black-filled natural rubber during fatigue measured by in-situ synchrotron X-ray diffraction, International Journal of Fatigue 47 (2013) 1–7.

[5] W. Busse, Tear resistance and structure of rubber, Rubber Chemistry and Technology 8 (1935) 122–137.

[6] N. Saintier, Fatigue multiaxiale dans un élastomère de type NR chargé: mécanismes d'endommagement et critère local d'amorçage, Ph.D. thesis, Ecole Nationale Supérieure des Mines de Paris (2001).

[7] T. Steinweger, U. Weltin, M. Flamm, Four tests to characterize a haigh-diagram for damage calculations, in: Constitutive Models for Rubber 4. Proceedings of the 4th European Conference on Constitutive Models for Rubber, ECCMR 2005 (Stockholm, Sweden, 27-29 June 2005), Vol. 4, Balkema, 2005, pp. 9–14.

[8] H. Oshima, Y. Aono, H. Nogushi, S. Shibata, Fatigue characteristics of vulcanized natural rubber for automotive engine mounts (characteristics of composition and mechanical properties), Memoirs of the Faculty of Engineering (Jyushu University) 67 (2007) 75–83.

[9] N. Saintier, G. Cailletaud, R. Piques, Cyclic loadings and crystallization of natural rubber: An explanation of fatigue crack propagation reinforce-

ment under a positive loading ratio, Materials Science and Engineering A 528 (2011) 1078–1086.

[10] E. Ostoja-Kuczinski, Comportement en fatigue des élastomères : application aux structures antivibratoires pour l'automobile, Ph.D. thesis, Université de Nantes / Ecole Centrale de Nantes (2005).

[11] M. Ludwig, T. Alshuth, M. El Yaagoubi, D. Juhre, Lifetime prediction of elastomers based on statistical occurrence of material defects, in: Constitutive Model for Rubber IX, Prague (Czech Republic), 2015.

[12] J. Marchal, Cristallisation des caoutchoucs chargés et non chargés sous contraintes : effet sur les chaînes amorphes, Ph.D. thesis, Université de Paris XI Orsay (2006).

[13] N. Candau, R. Laghmach, L. Chazeau, J. Chenal, C. Gauthier, T. Biben, E. Munch, Influence of strain rate and temperature on the onset of strain induced crystallization in natural rubber, European Polymer Journal 64 (2015) 244–252.

[14] K. Brüning, K. Schneider, S. Roth, G. Heinrich, Kinetics of strain-induced crystallization in natural rubber: a diffusion-controlled rate law, Polymer 72 (2015) 52–58.

[15] P. Kainradl, F. Händler, Heat build-up and destruction of vulcanizates under dynamic stress, Rubber Chemistry and Technology 28 (1955) 153–185.

[16] V. Le Saux, Y. Marco, C. Doudard, S. Calloch, P. Charrier, Fast evaluation of the fatigue lifetime of rubber-like materials based on a heat

build-up protocol and micro-tomography measurements, International Journal of Fatigue 32 (2010) 1582–1590.

[17] V. Le Saux, Y. Marco, S. Calloch, P. Charrier, D. Taveau, Heat build-up of rubber under cyclic loadings: validation of an efficient demarch to predict the temperature fields, Rubber Chemistry and Technology 86 (2013) 38–56.

[18] N. André, G. Cailletaud, R. Piques, Haigh diagram for fatigue crack initiation prediction of natural rubber components, Kautschuk und Gummi Kunststoffe 52 (1999) 120–123.

[19] A. Robisson, Comportement visco-hyperélastique endommageable d'élastomères SBR et PU: préediction de la durée de vie en fatigue, Ph.D. thesis, Ecole Nationale Supérieure des Mines de Paris (2000).

[20] F. Abraham, T. Alshuth, S. Jerrams, The effect of minimum stress and stress amplitude on the fatigue life of non strain crystallising elastomers, Materials & Design 26 (2005) 239–245.

[21] N. Saintier, G. Cailletaud, R. Piques, Multiaxial fatigue life prediction for a natural rubber, International Journal of Fatigue 28 (2006) 530–539.

[22] J. Poisson, F. Lacroix, S. Meo, G. Berton, N. Ranganathan, Biaxial fatigue behaviour of a polychloroprene rubber, International Journal of Fatigue 33 (2011) 1151–1157.

[23] E. Ostoja Kuczynski, P. Charrier, E. Verron, L. Gornet, G. Marckmann, Crack initiation in filled natural rubber: experimental database

and macroscopic observations, in: Constitutive Model for Rubber III, London (UK), 2003, pp. 3–10.

[24] T. Glanowski, V. Le Saux, C. Doudard, Y. Marco, C. Champy, P. Charrier, Proposition of an uncoupled approach for the identification of cyclic heat sources from temperature fields in the presence of large strains, Continuum Mechanics and Thermodynamics 29 (2017) 1163–1179.

[25] A. Medalia, Heat generation in elastomer compounds: causes and effects, Rubber Chemistry and Technology 64 (1991) 481–492.

[26] M. Flamm, T. Steinweger, U. Weltin, Cumulative damage in rubber materials, Kautschuk und Gummi Kunststoffe 55 (2002) 665–668.

[27] P. Charrier, Y. Marco, V. Le Saux, R. Ranaweera, On the influence of heat aging on filled NR for automotive AVS applications, in: Constitutive Model for Rubber VII, Dublin (Ireland), 2011, pp. 381–388.

[28] W. Kim, H. Lee, J. Kim, S. Koh, Fatigue life estimation of an engine rubber mount, International Journal of Fatigue 26 (2004) 553–560.

[29] T. Zarrin-Ghalami, A. Fatemi, Material deformation and fatigue behavior characterization for elastomeric component fatigue life predictions, Polymer Engineering and Science 52 (2012) 1795–1805.

[30] R. Luo, W. Mortel, X. Wu, Fatigue failure investigation on anti-vibration springs, Engineering Failure Analysis 16 (2009) 1366–1378.

[31] W. Mars, Multiaxial fatigue of rubber, Ph.D. thesis, University of Toledo (2001).

[32] Q. Li, J. Zhao, B. Zhao, Fatigue life prediction of a rubber mount based on test of material properties and finite element analysis, Engineering Failure Analysis 16 (2009) 2304–2310.

[33] B. Huneau, I. Masquelier, I. Marco, V. Le Saux, S. Noizet, C. Schiel, P. Charrier, Fatigue crack initiation in a carbon black-filled natural rubber, Rubber Chemistry and Technology 89 (2016) 126–141.

[34] S. Edwards, T. Vilgis, The effect of entanglements in rubber elasticity, Polymer 27 (1986) 483–492.

[35] V. Le Saux, Y. Marco, G. Bles, S. Calloch, S. Moyne, S. Plessis, P. Charrier, Identification of constitutive model for rubber elasticity from micro-indentation tests on natural rubber and validation by macroscopic tests, Mechanics of Materials 43 (2011) 775–786.